

Variability of winter extreme precipitation in Southeast China: contributions of SST anomalies

Ling Zhang · Frank Sielmann · Klaus Fraedrich ·
Xiuhua Zhu · Xiefei Zhi

Received: 1 September 2014 / Accepted: 19 January 2015
© Springer-Verlag Berlin Heidelberg 2015

Abstract Tropical SST anomalies are among the largest drivers of circulation regime changes on interannual time scales due to its characteristic heat capacity decay time scales. The circulation anomalies associated with extreme precipitation and the corresponding atmospheric response to SST anomalies are derived from ECMWF ERA-Interim reanalysis data by employing composite analysis and lagged maximum covariance analysis. Our results show that interannual variability of extreme winter precipitation in Southeast China is in close accordance with the interannual variability of total winter precipitation. Both are associated with similar abnormal circulation regimes, but for extreme precipitation events the circulation anomalies and moisture transport channels are significantly intensified. Two main moisture transport channels are captured: one extends from the North Indian Ocean through India and the Bay of Bengal to South China, and the other from the West Pacific Ocean through Maritime Continent and South China Sea towards South China, which are related to the preceding autumn SST patterns, El Niño and the Indian

Ocean dipole (IOD), respectively. El Niño (La Niña) SST anomalies induce anomalous anticyclonic (cyclonic) circulation over Philippine Sea, which is favorable (unfavorable) to warm and humid air transport to South China from the tropical West Pacific by southwesterly (northeasterly) anomalies. Under these circulations, northeasterlies of East Asian Winter Monsoon are weakened (strengthened) resulting in extreme precipitation to be more (less) frequent in Southeast China. During the positive (negative) IOD phase, abundant (reduced) moisture transport to South China from tropical regions through India and Bay of Bengal is observed due to weakened (strengthened) Walker circulations and abnormal anticyclonic (cyclonic) circulation over India, leading to a higher (lower) likelihood for extreme precipitation events in Southeast China. The underlying physical mechanisms can be explained by a simplified one-dimensional vorticity equation (Sverdrup balance).

Keywords Extreme winter precipitation · Interannual variability · El Niño · IOD

L. Zhang (✉) · K. Fraedrich · X. Zhi
Collaborative Innovation Center on Forecast and Evaluation
of Meteorological Disasters, KLME, Nanjing University
of Information Science and Technology, Nanjing, China
e-mail: ling.zhang@zmaw.de; lingzhang@nuist.edu.cn

L. Zhang · K. Fraedrich
Max Planck Institute for Meteorology, Hamburg, Germany

F. Sielmann
Meteorological Institute, Hamburg University, Hamburg,
Germany
e-mail: frank.sielmann@uni-hamburg.de

X. Zhu
KlimaCampus, Hamburg University, Hamburg, Germany

1 Introduction

Southeast China has frequently suffered from extreme weather and flood events with large impacts on human society. In 2005, 2008, extreme freezing rain and snow in Southern China resulted in a considerable loss of life and property (Dong 2007; http://en.wikipedia.org/wiki/2008_Chinese_winter_storms). Considering an old saying that a person standing with one foot on a hot stove and the other on a block of ice is comfortable on average, we could clearly understand, that monthly or seasonal averages smooth information details that characterize exactly those extremes which are usually responsible for phenomena

affecting many human and natural systems. With global warming there seems to be an enhanced likelihood for the occurrence of extreme events and, therefore, an increasing number of analyses have been dealing with extreme events in various relevant fields in the last decade (Sun and Yang 2012; Wang et al. 2000, 2008, 2013; Zhang et al. 2014a). Many efforts have been made to relate large-scale circulation anomalies to changes of climate on a regional scale. These severe impacts on one of the most densely populated regions of the world draws our attention to improving our knowledge about influential large-scale circulation anomalies, thus finding predictors with the potential for forecasting the probability for extreme precipitation well in advance. The first studies about ENSO influence on precipitation events worldwide are dating back to the early 1920s (Walker 1923, 1924). More recent works are from the 1980s (e.g. Rasmusson and Wallace 1983; Shukla and Paolino 1983; McBride and Nicholls 1983). However, most of the studies are dealing with general precipitation rather than with precipitation extremes. Moreover, since in the literature we found a one-sided focus on ENSO, we also want to draw the readers' attention to the Indian Ocean basin, that also reveals very pronounced SST anomaly patterns.

To quantify and to localize the involved mechanisms will be the main focus of this study, thereby providing long-range forecasters with some helpful guidelines for making seasonal or even multi-seasonal predictions of extreme precipitation. The underlying circulation patterns generating extreme precipitation are nearly identical to those associated with Southeast China precipitation in general. This detailed information can be represented by commonly used indices like (Zhang et al. 2011), for example, the number of heavy precipitation days (monthly count when precipitation exceeds 10 mm/day), number of very heavy precipitation days (monthly count when precipitation lies above 20 mm) and very wet days (monthly total precipitation from days beyond the 95th percentile), to mention merely three commonly used ones. The very wet days index is employed in our study.

The precipitation related large-scale atmospheric circulation patterns affecting Southeast China are influenced by continental and oceanic processes. For the interannual variability of precipitation in Southeast China several patterns have been demonstrated as influential, such as ENSO, Siberian High, East Asian Winter Monsoon, sea surface temperature (SST) of South China Sea and the strength and position of the East Asian trough (Zhou et al. 2009; Zhou and Wu 2010; Zhang et al. 2014b). Wang et al. (2000) and Huang et al. (2003) show that tropical SST anomalies are among the largest drivers of circulation regime changes on interannual time scales due to its characteristic heat capacity decay time scales. ENSO as the main pattern in the Pacific estimated and its impact on the East Asian climate

anomalies have undergone extensive and in-depth discussions (Wang et al. 2000; Wang and Zhang 2002; Wu et al. 2003; Zhou et al. 2009; Zhou and Wu 2010; Chou et al. 2009; Kim et al. 2013). Kumar et al. (2013) determined the fraction of monthly mean SST variability linearly related to the ENSO (Niño3.4) SST index to be around 15–20 %, in some regions exceeding 25 % (north of equator in western Pacific). And the relationship between the SST anomalies over tropical Pacific and the climate of South China has changed after the late 1970s (Ding et al. 2010; Li et al. 2010; Wang et al. 2012), which is partially associated with the tropical SST patterns shifting from “conventional” ENSO SST to ENSO Modoki-like conditions in recent three decades (Feng and Li 2011; Zhang et al. 2011).

The Indian Ocean Dipole (IOD) is another important contributor among the tropical SST patterns, accounting for 12 % of the tropical Indian Ocean (TIO) SST variability (Saji et al. 1999), usually developing in summer, maturing in autumn, and decaying in winter. IOD describes an aperiodic oscillation of sea-surface temperatures among the three phases “positive”, “neutral” and “negative”. The positive phase is characterized by greater-than-average sea-surface temperatures and greater precipitation in the western Indian Ocean region, whereas the negative phase corresponds with the opposite conditions, thus warmer water and greater precipitation in the eastern Indian Ocean, and cooler and drier conditions in the west (Ashok et al. 2001). A strong positive phase tends to cause severe droughts in the surrounding land areas of Indonesia and Australia (Saji et al. 1999). A study by Ummenhofer et al. (2009) demonstrated a significant correlation between, for example, the Federation Drought (1895–1902) and World War II drought (1937–1945) and Indian Ocean variability in terms of the IOD, and none with the Pacific Ocean conditions as traditionally assumed. In this paper we want to add one further region possibly being affected by the IOD, namely South East China. Previous work has shown, that positive IOD events induce a stronger South Asian High, with an eastward-extending position and a strengthened Western Pacific subtropical high, and with a westward-extending position (Li and Mu 2001; Li et al. 2006; Yuan et al. 2008; Xie et al. 2009), which leads to precipitation anomalies in East China and causes extremely hot and dry summers in South China by generating a Rossby wave train (Guan and Yamagata 2003).

Based on the close relationship between tropical SST and East Asian climate anomalies, the atmospheric response to the SST anomalies, which is associated with the interannual variability of extreme precipitation in Southeast China, is investigated in our study. The paper is structured as follows: data and methods as well as a short description of the general circulation model (GCM) used to support the dynamical mechanisms are described in Sect. 2; the interannual

variability of Southeast China winter extreme precipitation and the associated SST-atmospheric circulation feedbacks are analyzed in Sect. 3; the responses of the associated circulations with Southeast China winter extreme precipitation anomalies to the tropical SST anomalies are presented in Sect. 4; the conclusion follows in Sect. 5.

2 Data and methods

2.1 Observations

Daily precipitation station observations in China are obtained from the National Meteorology Information Center, China Meteorological Administration, CMA. In this study we focus on Southeast China covering the region 20°N–35°N and 102.5°E–122.5°E, where high quality data from 229 stations are available from 1979 to 2013. The winter average value in this paper is taken from December of the previous year to February of the current year, such as the average value taken from the winter of 1979/1980 (the winter of 1980 for short in this paper) refers to that from December 1979 to February 1980. The extreme precipitation of each station was defined by the 95th percentile with respect to daily precipitation (above 0.1 mm) from winter 1980 to 2013. Extreme precipitation days are defined by a binary index representative for Southeast China, which is set to 1 for a day with at least 10 % of stations with extreme precipitation exceeding the 95th percentile threshold and otherwise it is set to 0, then calculating how many days of each winter season. All circulation related meteorological fields and the global SST are taken from the ECMWF ERA-Interim reanalysis (2006 version of the ECMWF Integrated Forecast Model IFS Cy31r2; Dee et al. 2011).

Large-scale atmospheric response to SST anomalies has been studied by methods that determine the key SST patterns, such as the lagged maximum covariance analysis (MCA), generalized equilibrium feedback assessment (GEFA) and maximum response estimation (MRE) (Czaja and Frankignoul 1999; Czaja and Frankignoul 2002; Frankignoul and Kestenare 2005; Frankignoul et al. 2011). Frankignoul et al. (2011) compared these multivariate statistical methods, showing that GEFA is less robust and sensitive to the truncation. MRE and MCA are generally robust and essentially unbiased, but MRE is more sensitive to sampling errors. MCA is chosen in this study with regard to the other methods' sampling limitations and truncation issues, and finally the MCA also provides the most robust estimates of the largest atmospheric responses (Frankignoul et al. 2011). The statistical significance of MCA modes are estimated using the bootstrap approach with 100 random samples (von Storch and Zwiers 1999; Czaja and Frankignoul 2002).

Due to ENSO and IOD mutual interaction and co-contributions to precipitation anomalies (Yuan and Yang 2012), linear regression is applied to remove the ENSO or IOD signals, respectively, from SST and associated atmospheric data. For example, in order to highlight the winter atmospheric responses to the relative pure IOD (El Niño) SST patterns, SST anomalies in the Indian (Pacific) basin and associated atmospheric circulation fields have been reduced by the El Niño (IOD) contributions by subtracting the original SST anomaly linearly regressed with Niño 3.4 (IOD) index. Composite analysis and student's *t* test are employed to further examine the mechanisms between associated circulation anomalies of anomalous extreme precipitation in Southeast China and SST patterns. Niño 3.4 index is used to describe El Niño events, which is defined by the SST averaged over (5°S–5°N, 170°W–120°W) in winter. IOD index is defined by the SST differences between the western (10°S–10°N, 50°E–70°E) and the eastern (10°S–0°, 90°E–110°E) regions of Indian Ocean (Saji et al. 1999) in autumn.

2.2 Model

In order to confirm the role of SST anomalies in driving abnormal moisture channels during autumn and winter, the GCM 'PlaSim' (Fraedrich et al. 2005; Fraedrich 2012; Dahms et al. 2011; Schmittner et al. 2011) is employed to conduct SST forcing experiments. PlaSim is a spectral GCM, whose dynamical core for the atmosphere is adopted from Portable University Model of the Atmosphere (PUMA), which is freely available for download at <http://www.mi.uni-hamburg.de/plasim>. The model is based on the moist primitive equations conserving momentum, mass, energy and moisture. Besides the atmospheric part, other climate subsystems are included with highly reduced dynamics: a land surface with biosphere and a mixed layer-ocean with sea ice. A detailed overview of the PlaSim climatology can be found at http://www.mi.uni-hamburg.de/fileadmin/files/forschung/theomet/docs/pdf/PS_Climate_Report.pdf. The horizontal resolution used in this study is T42 (~2.8° × 2.8°) with ten vertical sigma levels. The statistical significance of the climatological differences between control run and sensitivity run is estimated by the small-sample test (Preisendorfer and Barnett 1983; Zhi 2001).

3 Climatological features of extreme precipitation in Southeast China

3.1 Climatological setting

The climatological mean, the winter to winter variances and the EOF analysis of winter precipitation in Southeast

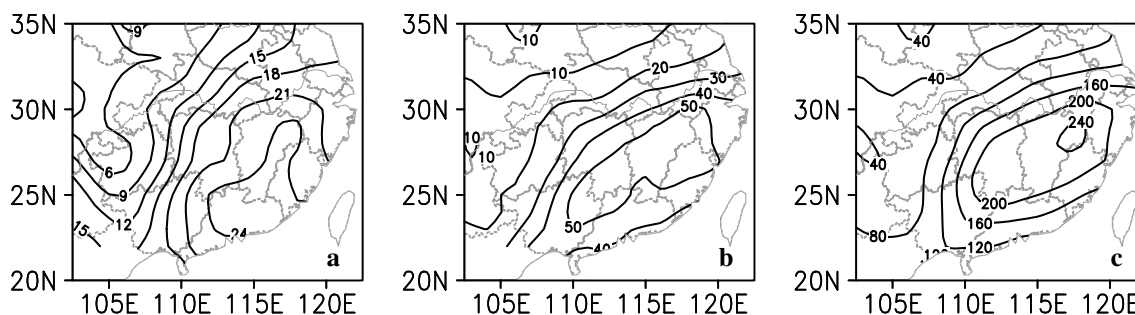


Fig. 1 Geographical distributions: **a** 95th percentile threshold of daily winter (De.c–Feb.) precipitation (in mm per day); **b** climatological mean of annual sums of winter extreme precipitation (in mm per winter) and **c** general precipitation (in mm per winter) for 1980–2013

China show abundant precipitation with maximum values above 210 mm/winter and a uniform monopole pattern over Southeast China (Zhang et al. 2014a). In our study the extreme precipitation events are defined by exceedance of the 95th percentile threshold. The thresholds of extreme precipitation in Southeast China are shown in Fig. 1a. Note that, regarding the thresholds, the climatological mean of annual sums of extreme precipitation in Southeast China show a similar pattern as the distribution of annual sums of winter total (general) precipitation, with maximum in the south of the Yangtze River (Fig. 1b, c). On average, winter extreme precipitation accounts for 20–30 % of total precipitation in most parts of Southeast China.

In the following we employ composite analysis to examine circulation anomalies associated with winter extreme precipitation in Southeast China. Extreme precipitation days are defined as those days with at least 10 % of stations in Southeast China having extreme precipitation in terms of exceeding the 95th percentile threshold. Thereby we obtain 139 winter extreme precipitation days in Southeast China during 1980–2013. According to these criteria, the geographical distribution of extreme precipitation in Southeast China (not shown) shows a similar pattern as the Fig. 1b (the extreme precipitation events are defined by exceeding the 95th percentile threshold), but with higher maximum values. This indicates that the criterion for extreme precipitation days is a suitable index for further analyses of the extreme precipitation events in Southeast China. Based on this index (EPD: extreme precipitation days index; black solid line in Fig. 4), the associated larger-scale circulation regimes are analyzed by composite analysis.

3.2 Composites

Winter near surface atmospheric circulation over the Eurasian continent is dominated by the Siberian High (Gong and Wang 1999; Gong and Ho 2002). Northeast China is located under the eastern part of the Siberian High where northwesterlies prevail, while the southeast coast of China

is under the influence of the southeastern part of the Siberian High, where northeasterlies prevail. The horizontal wind anomalies at 10 m (Fig. 2a) indicate that anomalous southerlies prevail over the southeast coast of China and South China Sea and from India to Southwest China that is controlled by anomalous westerlies during Southeast China extreme precipitation days. This demonstrates that East Asian Winter Monsoon (EAWM) is weakened over mid- to low latitudes and southward intrusion of cold air from the north is suppressed. Meanwhile, warm and humid air from Indian Ocean is transported to South China by abnormal westerlies. The moisture transport anomalies are further analyzed by a vertical integral of water vapour flux (Fig. 2b). Two major transport channels are observed: one extends from the North Indian Ocean through India and the Bay of Bengal to Southwest China, and the other from the West Pacific Ocean through the South China Sea towards South China. These abnormal moisture transports are directed northward with warm humid air from tropical oceans contributing to positive moisture anomalies in the southeast coast of China, where it meets cold air from the north, thus water vapour convergence (Fig. 3a) leads to anomalous precipitation.

In order to highlight the atmospheric circulation features of extreme precipitation events, the circulation composites of general precipitation events are analyzed as reference. The precipitation day definition is similar to that of the extreme precipitation day: when 10 % of stations in Southeast China have a daily precipitation exceeding 0.1 mm/day, this day is defined as Southeast China precipitation day. Thereby we get 2,129 winter precipitation days in Southeast China during 1980–2013. Regarding to this criteria, the geographical distribution of general precipitation in Southeast China (not shown) shows almost the same pattern as the Fig. 1c (precipitation events are defined by exceeding 0.1 mm/day), which demonstrates that the precipitation day is a useful index for winter precipitation in Southeast China. Based on this index (PD: precipitation days index; grey solid line in Fig. 4), the associated larger-scale circulation regimes are analyzed by

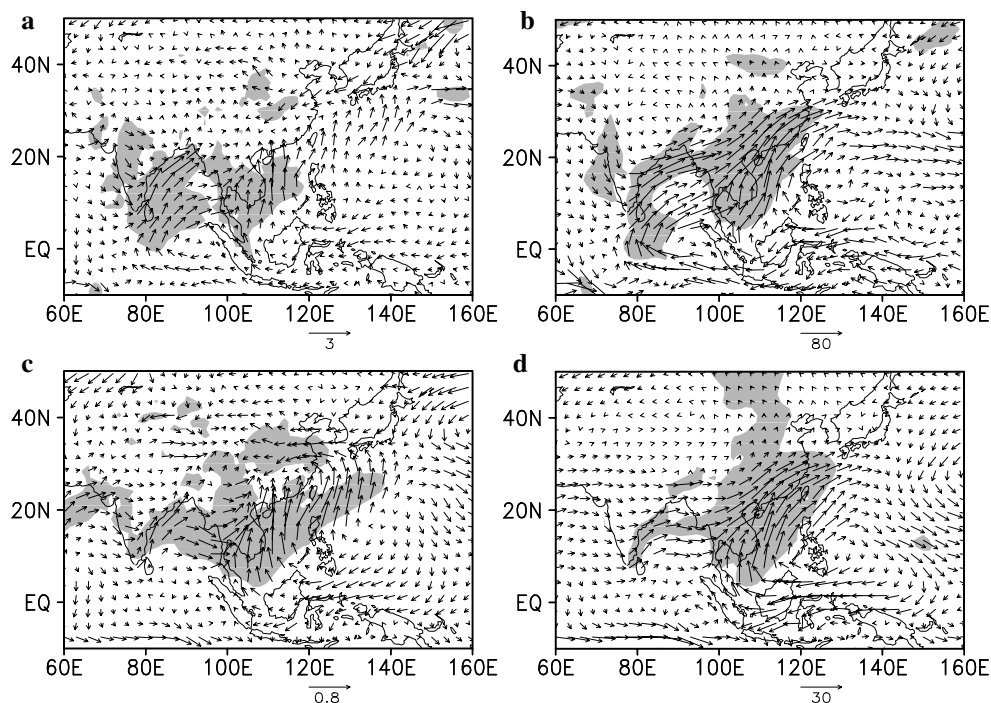
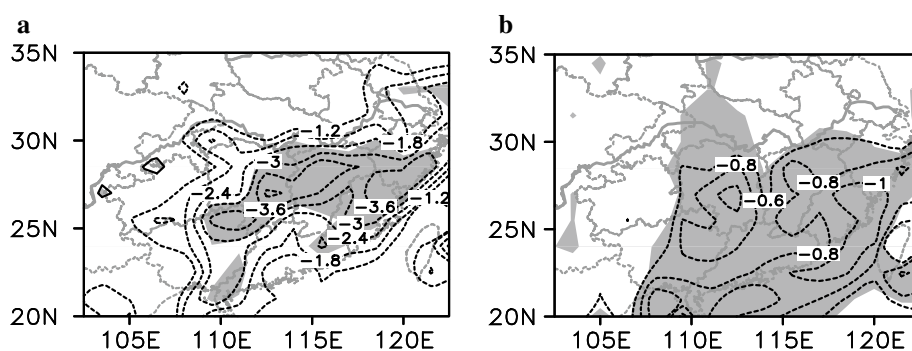


Fig. 2 Composite map for days with at least when 10 % of stations in Southeast China having extreme precipitation in terms of exceeding the 95th percentile threshold and *shaded areas* are statistically significant at 95 % confidence level: **a** mean extreme event horizontal

wind anomalies at 10 m (m/s); **b** vertical integral of water vapour flux anomalies for extreme events [$\text{kg}/(\text{m s})$]; **c** and **d** are same as **a** and **b**, but for all precipitation events

Fig. 3 The same as Fig. 2, but for **a** vertical integral of divergence of moisture flux anomalies for extreme events ($10^{-5} \text{ kg m}^{-2} \text{ s}^{-1}$); **b** is same as **a**, but for all precipitation events



composite analysis. The circulation composites of all precipitation events show a similar pattern as that of the extreme cases with weaker intensity (Figs. 2c, d, 3b). That is, extreme precipitation events have a close relationship with the large scale background circulation. From Fig. 2a–d we can further conclude that extreme winter precipitation in Southeast China is primarily advective, although the individual precipitation event itself is convectively triggered.

The annual sums of extreme winter precipitation days and winter precipitation days show the interannual variability of extreme and total precipitation in Southeast China (Fig. 4). The interannual variability of extreme precipitation is in good accordance with that of total precipitation, especially during mid of 1980s–early of 2000s, indicated by a correlation of 0.59 between annual sums of EPD and PD.

This further supports our hypothesis that extreme precipitation events are favored by the same underlying circulation anomalies as total precipitation events; that is, by the same dynamical mechanisms associated with the interannual timescale. Its intensities, however, are determined by both local thermodynamics as well as moisture supply on the interannual timescale.

4 Atmospheric response to SST anomalies

As mentioned before, a majority of studies have analyzed the role of the SST to modulate large-scale atmospheric flow patterns and secondly as one driver for moisture release on a variety of time scales, and thus indirectly

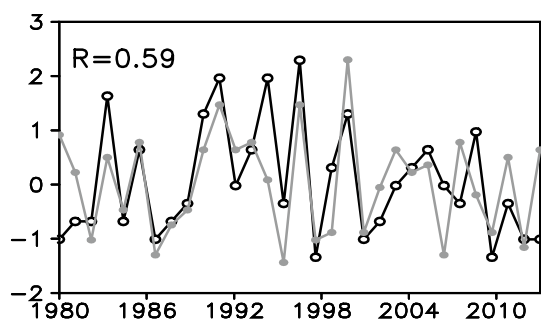


Fig. 4 Annual sums of extreme winter precipitation days (*black solid line*) and winter precipitation days (*grey solid line*) according to extreme precipitation days index (EPD) and precipitation days index (PD); all values are normalized. $R = 0.59$ is the correlation coefficient between EPD and PD

its impact on precipitation. In order to get a first hint of involved SST anomaly patterns, we carried out a grid point-wise correlation between the SST of the Indian/Pacific Ocean and the EPD time series. Two centers of action are identified, indicated by high correlations (not shown): These are the ENSO pattern in the early (autumn) stage and an IOD pattern in the Indian Ocean with a weak negative pole.

The high correlation of 0.62 between IOD and Niño 3.4 index in autumn reflects the fact that there is a 30 % co-occurrence of IOD and El Niño events, which does not necessarily mean that these two phenomena are causally connected in the physical space (Vinayachandran et al. 1999; Rao et al. 2002; Guan and Yamagata 2003; Yamagata et al. 2013; Ashok et al. 2003). This partial coupling of IOD and ENSO was also addressed by Clarke and Liu (1993) and Meyers (1996), explaining the ENSO influence through an intruding of a coastal oceanic wave-guide around the Australian continent into the eastern Indian Ocean, originating in the western Pacific. The anomalous (weakened) Walker cell, the driving factor for the anomalous equatorial easterly moisture transport, could be shown as exclusively existing during pure IOD events (Fig. 8 and Fig. 4 in Yamagata et al. 2003). However, the local effect of ENSO through the Clarke-Meyers-effect (Clarke and Liu 1993; Meyers 1996) effect contributes to the overall IOD-ENSO correlation

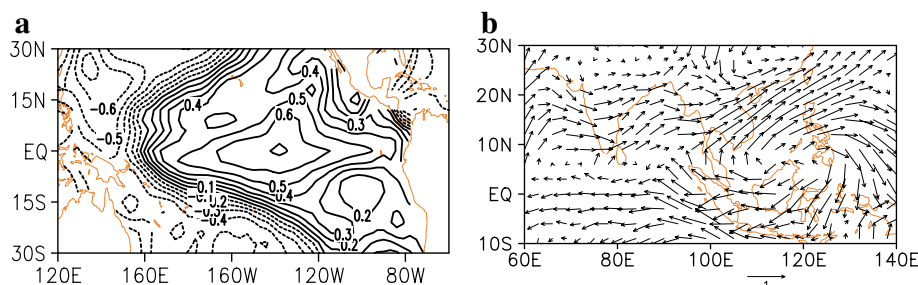
during boreal fall. Therefore, in our study, in order to highlight the winter atmospheric responses to the relative pure IOD (El Niño) SST patterns, SST anomalies in the Indian (Pacific) basin and associated atmospheric circulation fields have been reduced by the El Niño (IOD) contributions by subtracting the original SST anomaly regressed with Niño 3.4 (IOD) index.

Since the ordinary correlation analysis does not discriminate dominating from non-dominating simultaneous patterns, we perform a lagged MCA separately with the Pacific SST and tropical Indian SST, and an atmospheric field representing the large-scale moisture channels, which is the vertically integrated water vapour flux. The MCA finds two (or more) highly correlated patterns ranked according to their contributions to the total variance (explained variance) as analyzed next.

4.1 Response to tropical Pacific SST

To investigate how the tropical Pacific SST influences the associated moisture channels and winter precipitation in Southeast China, MCA was applied to the preceding autumn SST over (30°S – 30°N , 120°E – 60°W) and the vertically integrated moisture flux over (10°S – 30°N , 60°E – 140°E) of the subsequent winter. In this section all fields have been diminished by the IOD contributions through subtracting the original fields regressed with the IOD index. MCA isolates coupled pairs of spatial patterns and their associated time series by performing a singular value decomposition of cross-covariance matrices between two fields. The statistical significance of each pattern was tested in terms of squared covariance and the correlation between the MCA time coefficient series of two fields. Figure 5a, b shows the maximum covariance patterns of the first MCA mode between the preceding autumn tropical Pacific SST and the vertically integrated water vapour flux. The patterns are significant at 95 % confidence level and explain 58.68 % of total covariance. The correlation between the MCA time coefficients of the two fields is 0.77. As the second mode is not significant only the first mode is presented showing an anomalous anticyclone over the Philippines in conjunction with anomalous moisture

Fig. 5 Covariance maps of the first MCA mode with **a** tropical Pacific SST anomalies over (30°S – 30°N ; 120°E – 60°W) in preceding autumn and **b** the subsequent winter mean vertical integral of water vapour flux



transports to the southeast coast of China by southwesterlies, associated with abnormal central-eastern Pacific warm and western Pacific cool (positive phase in our study).

To illustrate the common non-linear characteristics of the tropospheric moisture transport anomalies during the positive (negative) phase of SST anomalies, composite analysis is employed. These are composite maps of seasonal circulation anomalies from preceding autumn to winter, respectively. Anomalous positive (negative) years are defined, when the standardized MCA time coefficients of the Pacific SST are greater (less) than 1 (−1). This defines the preceding autumn tropical Pacific SST abnormal positive phase years, including 1983, 1987, 1988, 1993, 1994 and abnormal negative phase years comprising 1989, 1999, 2000, 2001, 2008, 2009. During the positive SST anomalies' years (left column in Fig. 6), warming SST is shown in the central-eastern Pacific with maximum values in the central Pacific in the fall (Fig. 6a) and winter (Fig. 6c). And the Walker circulation over western-central Pacific is strengthened by the abnormal SST forcing (Fig. 6i, k), which is characteristics of anomalous ascending (descending) motion over central (western) Pacific. The composites of the vertically integrated water vapour flux in autumn (Fig. 6e) show water vapour transport from North India through South Asian to Southeast China and, furthermore, abnormal divergences of the vertically integrated water vapour flux (not shown) occur in South Asia while anomalous convergences are noted in Southeast China during SST abnormal positive phase years. The typical associated anticyclonic circulation over Philippines with El Niño cannot be shown clearly in the autumn mean circulations, because it establishes itself in October and, with increasing amplitude, shifting to the Philippines in November (Wang and Zhang 2002). In winter (Fig. 6g), the anticyclonic circulation remains over the Philippines with moisture flux divergence over the tropical western Pacific and maritime continents and convergence over the east coast of China during the positive phase years of tropical Pacific SST. It coincides with abundant moisture from tropical western Pacific being transported to Southeast China through the maritime continents, South Asia and South China Sea by the anticyclonic circulation over Philippines.

Wang et al. (2000) studied Pacific-East Asian teleconnections by reanalysis data and modelling of the atmospheric general circulation. They found that the abnormal Philippine anticyclone results from the Rossby-wave response being reduced by suppressed convective heating, which, in turn, is induced by a positive El Niño pattern with central-eastern Pacific warming and western Pacific cooling. That is, the anomalous Philippine anticyclone originates from the positive thermodynamic feedback of western Pacific cooling through local convective heating decrease (Wang and Zhang 2002). This mechanism explains the

relationship between the positive El Niño SST pattern and the anomalous Philippine Sea anticyclone (PSAC) as supported by our MCA and composite analyses. Positive El Niño SST anomalies induce anomalous anticyclonic circulations over Philippine, leading to prevailing southwesterlies over Southeast China. These circulation conditions weaken the northeasterlies of the EAWM and favor warm and humid air transport to Southeast China, resulting in more frequent extreme precipitation. We can conclude that autumn Pacific SST anomalies may be skillfully used as a major predictor for forecasting winter precipitation anomalies in Southeast China. Here, it should be noted that several other mechanisms have been identified contributing to the establishment and maintenance of the PSAC (Wang and Zhang 2002; Takaya and Nakamura 2013). Wang and Zhang (2002) found that the deepening of the upper-level East Asian Trough in conjunction with cold air intrusions to the Philippines supports the formation of PSAC via subsidence and further SST cooling. Hence, modulations of planetary waves on interannual scales may play a role, as suggested for the variability of the EAWM (Takaya and Nakamura 2013).

4.2 Response to tropical Indian SST

Since the end of the last century, the so-called IOD mode has been considered as another important—besides ENSO—aperiodic oscillation of sea-surface temperatures, alternating among “positive”, “neutral” and “negative” phases. The positive phase is characterized by greater-than-average sea-surface temperatures and greater precipitation in the western Indian Ocean region, whereas the negative phase corresponds with the opposite conditions, thus warmer water and greater precipitation in the eastern Indian Ocean, and cooler and drier conditions in the west (Saji et al. 1999).

4.2.1 Observations

In order to highlight the effects of IOD on the associated circulation anomalies with winter precipitation in Southeast China in this section, all fields have been reduced by the El Niño contributions by subtracting the original fields regressed with the Niño 3.4 index. This corrected Indian Ocean SST over (30°S–30°N, 30°E–120°E) is subjected to MCA analysis with the vertically integrated moisture flux over (10°S–30°N, 60°E–140°E). The first mode, which explains 37.8 % of the total covariance, shows SST Indian basin mode, but the corresponding moisture flux patterns do not appear to be closely related to the winter precipitation variability of Southeast China (not shown). The second mode (Fig. 7), which explains 21.3 % of the total covariance and reaches statistical significance at 90 % confidence

Fig. 6 Composites of seasonal mean anomalies of SST ($^{\circ}\text{K}$, **a–d**), vertical integral of water vapour flux ($\text{kg}/(\text{m s})$, **e–h**) and the meridional-height section of longitude mean of zonal wind (U , m/s) and vertical velocity (W , Pa/s) along (-4.5°S to 4.5°N) (**i–l**) in fall and winter during positive (*left*) and negative (*right*) central-eastern Pacific abnormal years and shaded areas are statistically significant at 95 % confidence level; vertical velocity is multiplied with -100 to get positive results with adjustment to the u scale

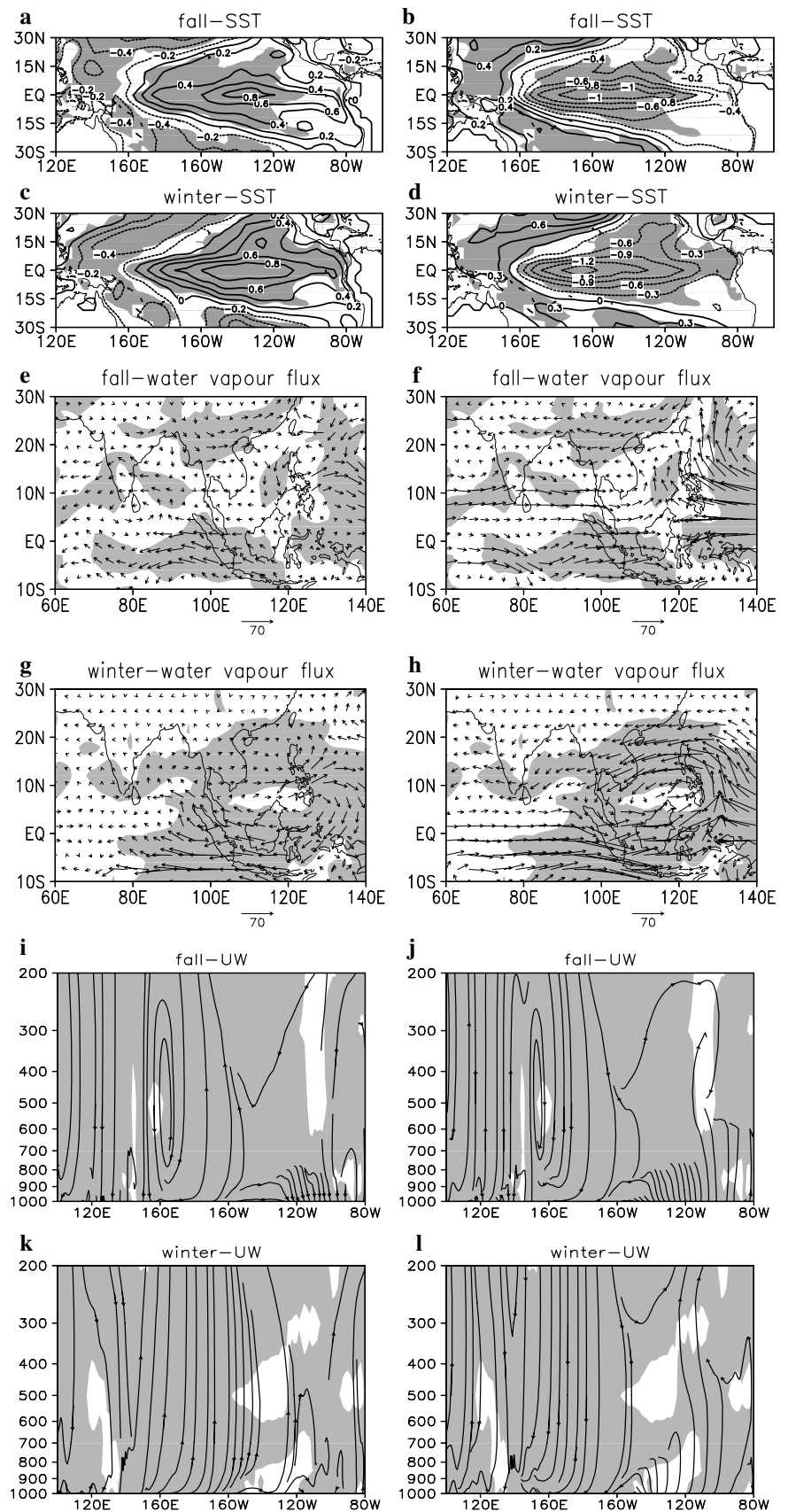
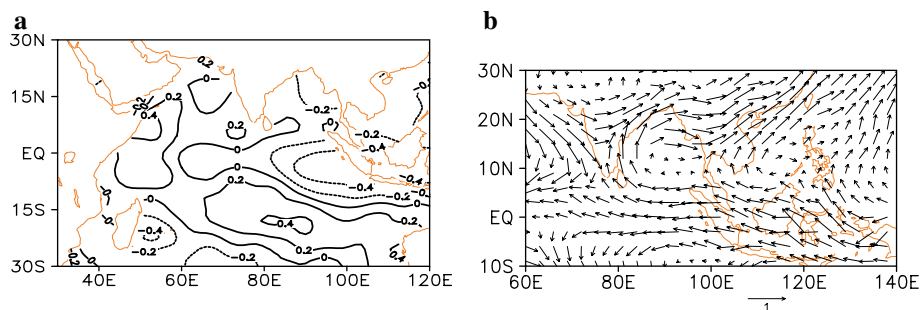


Fig. 7 Covariance maps of the second MCA mode with **a** tropical Indian SST anomalies over (30°S–30°N; 30°E–120°E) in preceding autumn and **b** the subsequent winter mean vertical integral of water vapour flux



level, shows the SST IOD mode; the correlation between the second mode time coefficients of SST and the horizontal vertically integrated water vapour flux is 0.79. The anticyclonic circulation anomalies show up over South China Sea, which favor moisture transport to South China from Maritime Continents and the adjacent sea during the IOD events. Simultaneously we observe abnormal easterlies prevailing near the equator, which turn northward to the Indian continent and merge into westerly anomalies over northern India. This abnormal atmospheric circulation conveys abundant moisture from the Indian Ocean to South China through the Bay of Bengal. During IOD events these two moisture channels are favorable to winter precipitation increase in Southeast China.

Composite analysis is applied to illustrate the common characteristics of the moisture flux and vertical circulation anomalies' evolution during the positive (negative) phase of IOD (Fig. 8). Anomalous positive (negative) years are defined when the standardized MCA time coefficients of the second mode of Indian SST are greater (less) than 1 (−1). Thereby we get IOD positive phase years (cooling in the East Indian Ocean and warming in the West Indian Ocean) in preceding autumn including 1983, 1989, 1995, 1998, 2008 and IOD negative phase years (warming in the East Indian Ocean and cooling in the West Indian Ocean) in preceding autumn comprising 1993, 1999, 2005, 2006. During positive phase years of IOD (left column in Fig. 8), SST negative anomalies appear in the East Indian Ocean and positive anomalies show up in the Central-west Indian Ocean in the autumn (Fig. 8a). And the negative SST anomalies disappear in the winter, but the positive SST anomalies still maintain in the South of TIO (Fig. 8c). In the atmosphere, easterly anomalies prevail near the equator of Indian Ocean and southerly anomalies appear over west India, turning eastward over North India and transporting moisture to Southeast Asia and South China Sea through Bay of Bengal in preceding autumn (Fig. 8e). The anticyclonic circulation over India is obvious in autumn (Fig. 8e) and moving east to the Bay of Bengal in winter (Fig. 8g). The vertically integrated divergence of water vapour flux shows abnormal divergence over North Indian Ocean and convergence over Southeast China in winter (not shown). It

implies that the Indian moisture channel favors warm and humid air transport from TIO to Southeast Asia and Southeast China through the Bay of Bengal in winter which, at the same time, weakens the EAWM. In addition, an anti-Walker circulation is observed over the TIO with descending motion over East Indian Ocean, ascending motion over West Indian Ocean and easterlies over equator of Indian Ocean in autumn (Fig. 8i) and winter (Fig. 8k). During the negative IOD phase (right column in Fig. 8), warming anomalies in the East of Indian Ocean and cooling anomalies in the Central-west Indian Ocean are observed in the autumn (Fig. 8b). And the atmospheric circulation anomalies are not as relevant for South China precipitation as those of the positive phase, but there are slightly intensified northerlies in South China, which still can be observed in fall (Fig. 8f) and winter (Fig. 8h). It implies that the negative phase of IOD increases the intensity of EAWM leading to a colder and drier winter in Southeast China.

The effects of IOD on Southeast China precipitation are mainly based on Indian Ocean anomalous moisture channels. The Maritime continent channel, captured clearly by MCA analysis, does not appear to be statistically significant in the composite analysis. The Walker circulation over the Indian Ocean is weakened by a cooling of the East Indian Ocean and a warming of the West Indian Ocean (positive phase of IOD) leading to easterly flow anomalies in equatorial regions (double green straight arrows in Fig. 10). And the anticyclonic circulation anomalies over India are caused by the cooling of the East Indian Ocean. The anomalous cooling over East Indian Ocean excites equator-symmetric Rossby waves (Fig. 9 shading), which enhances the low level anticyclonic circulations on the western margins of the cooling zone due to planetary wave propagation. This phenomenon is confirmed by the anomalous sea level pressure and stream function (Fig. 9 black solid lines and shadings) over India and the South Indian Ocean.

The mechanism of a heat-induced tropical circulation can be explained by a simplified shallow-water model (Gill 1980; Philips and Gill 1987) as follows: Friction is set to zero, leading to a vorticity equation analog to the Sverdrup equation in oceanography, written as $\beta v = f \partial w / \partial z$ (with meridional wind speed v , Coriolis parameter f and vertical

Fig. 8 Composites of seasonal mean anomalies of SST ($^{\circ}\text{K}$, **a–d**), vertical integral of water vapour flux ($\text{kg}/(\text{m s})$, **e–h**) and the meridional-height section of longitude mean of zonal wind (U , m/s) and vertical velocity (W , Pa/s) along (-4.5°S to 4.5°N) (**i–l**) in fall and winter during positive (*left*) and negative (*right*) Indian Ocean Dipole (IOD) phase years and shaded areas are statistically significant at 95 % confidence level; vertical velocity is multiplied with -100 to get positive results with adjustment to the u scale

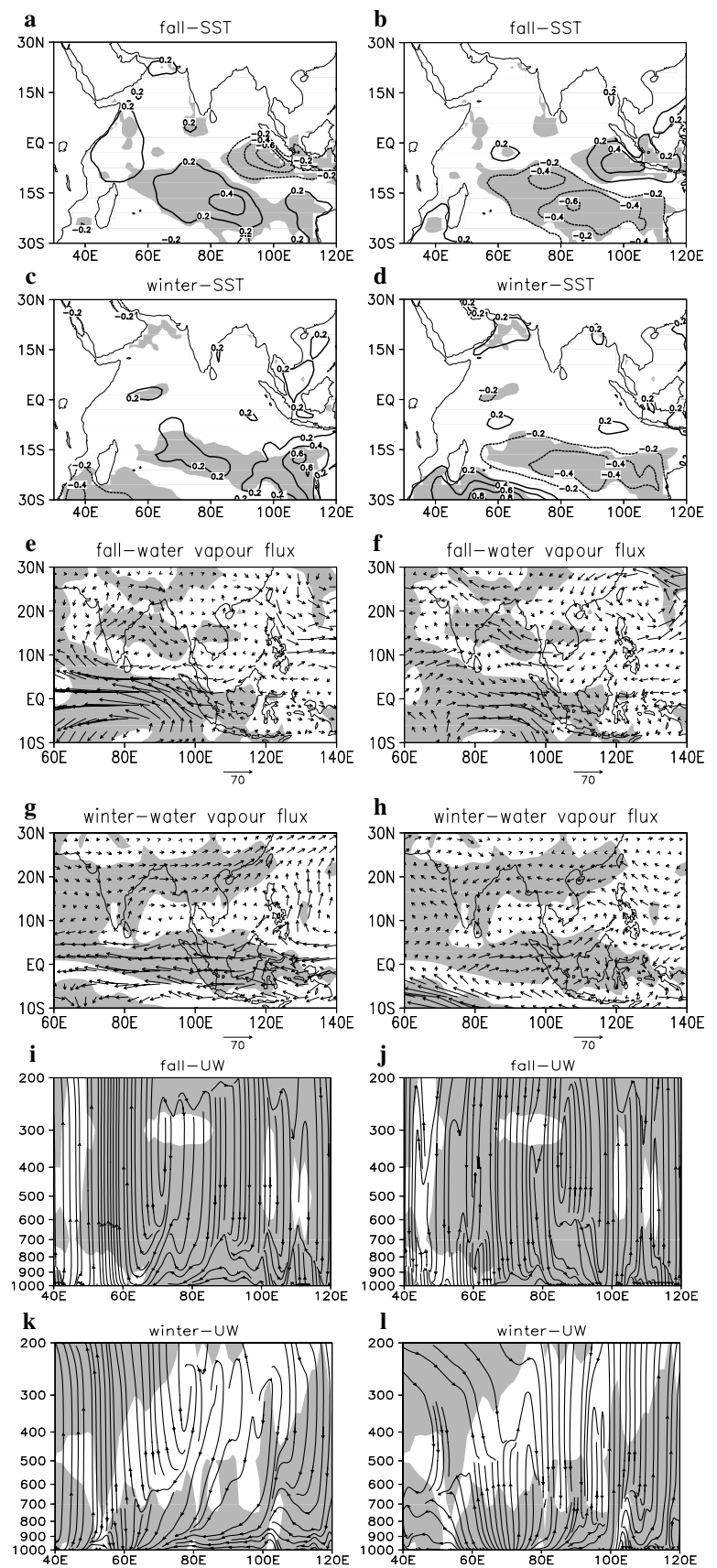


Fig. 9 Composites of seasonal mean anomalies of sea level pressure (black solid lines, Pa) and stream function (shading, $10^7 \text{ m}^2/\text{s}$) at 850 hPa in fall (a) and winter (b) with positive Indian Ocean Dipole (IOD) phase years

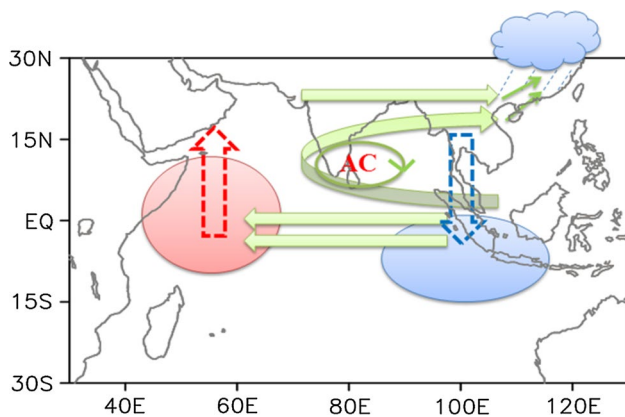
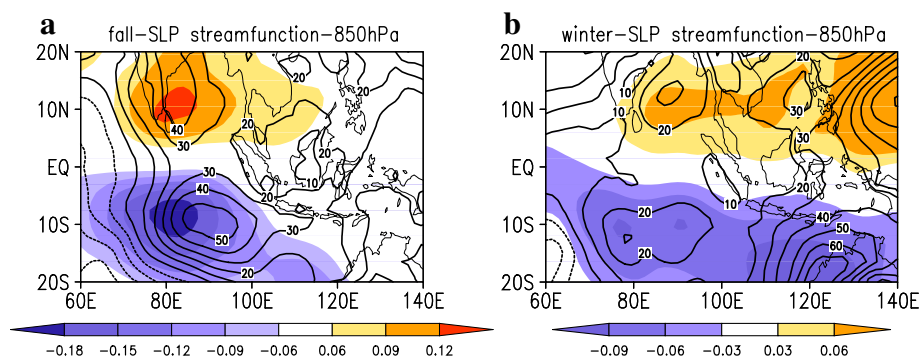


Fig. 10 Sketch map of circulation anomalies associated with IOD. Red/blue shaded areas indicate positive/negative SST anomalies. Dashed red/blue arrows correspond to ascending/descending motions. Green arrows indicate the horizontal circulation anomalies. AC represents the anomalous anticyclone. The heat induced equatorial easterly anomaly during the positive IOD phase transports abundant moisture from the equatorial regions westward. Its northward turn, that can be interpreted as a draw-off branch of the strong zonal-equatorial ‘moisture highway’ (double green arrow) to South China through the Indian Ocean, North India and the Bay of Bengal, is modulated by abnormal anticyclonic circulations (AC) over India and Bay of Bengal as a result of cooling in the East Indian Ocean (blue shading). Consequently the EAWM weakens, which, in turn, leads to extreme precipitation events to be more likely to occur in Southeast China

wind speed w). For $\partial w/\partial z$ negative in the lower level, the air column is squeezed, losing vorticity and particles move to lower latitudes ($v < 0$, symbolized by a small green arrow on the eastern flank of the anticyclone AC in Fig. 10), where the background vorticity is identical to the column vorticity (smaller f), satisfying the zero friction assumption. This indicates that northerlies are induced near the cooling source, creating the eastern flank of the anticyclone. With Rossby wave speed c and the meridional derivation of the Coriolis parameter $\beta = \frac{df}{dy}$, the size of the anticyclone given by the Rossby radius $(c/2\beta)^{1/2}$, is typically about 1,000–1,500 km diameter. The poleward flow is roughly located at the western flank of the anticyclone (due to planetary wave propagation) which, merging into westerly anomalies over

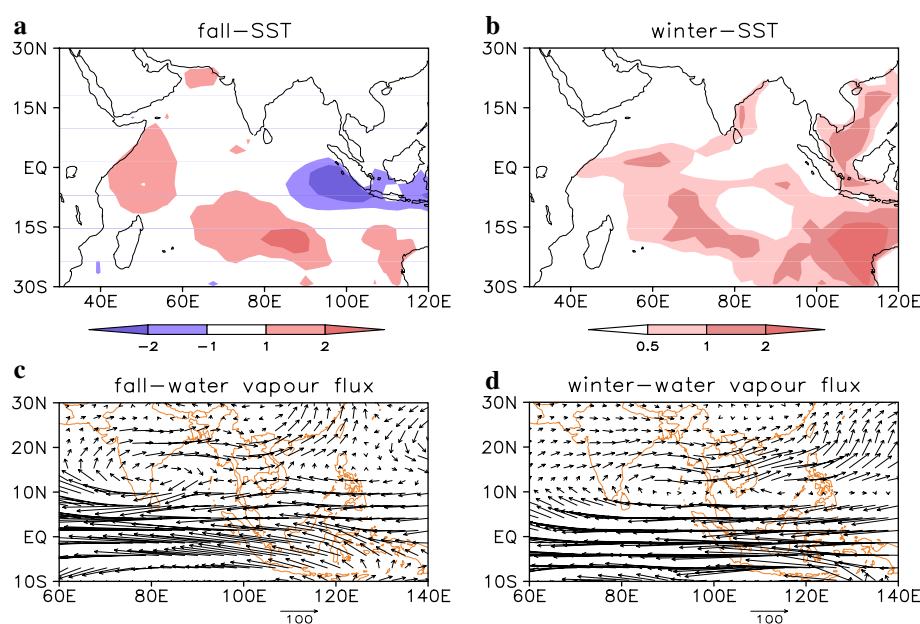
the subtropical region (green straight arrow in Fig. 10), positions the anticyclone over south India (AC in Fig. 10). In the winter, heat differences between East TIO and Central TIO still exist due to the significant warming in the central-south of tropical Indian Ocean, which maintains abnormal easterlies over equatorial Indian Ocean. In meridional direction, the poleward flow over India is maintained by the heat differences between North and South tropical Indian Ocean. Under these heating conditions, the abnormal anticyclonic circulation maintains over North Indian Ocean. Easterly propagating planetary waves during winter due to high level (>500 hPa) westerly background flow transport abnormal anticyclonic vorticity eastward, moving the anomalous anticyclonic circulation to the East of India and Bay of Bengal. Hence, the Indian Ocean anomalous moisture channel (green broad curved arrows in Fig. 10) in winter is the result of the abnormal heating pattern over the Indian Ocean. For the negative IOD phase, the circulation anomalies are almost symmetric with IOD positive phase years, but less intense.

4.2.2 Modeling

A SST forcing experiment with PlaSim (Fraedrich et al. 2005) GCM is employed to investigate the role of TIO SST anomalies in driving abnormal moisture channels during autumn and winter. A climatological global Atmospheric Model Intercomparison Project (AMIP) SST with annual cycle is applied as SST forcing in the control run. The last 30 years of a 50 years control run were used in our study. The forcing experiment has run 30 years with the same set up after a spin-up time of unforced 50 years, with abnormal SST added to the climatological SST forcing. The abnormal SST is derived from the composites of seasonal mean anomalies of the ERA-Interim SST (Fig. 8a, c), multiplied with five times the amplitude for better atmospheric responses (Fig. 11a, b).

The differences between abnormal SST forcing and control simulation are shown in Fig. 11c, d. The following features of the observational diagnostics are captured:

Fig. 11 The abnormal tropical Indian Ocean (TIO) SST forcing (a, b; °K) and the differences of the vertical integral of water vapour flux between TIO sensitivity experiment and control simulations [c, d; kg/(m s)] during fall and winter. The difference fields are significant at 95 % confidence level



The anticyclonic circulation over South India occurs in response to the cooling over tropical Indian Ocean in fall, which is established poleward upstream of the cooling region (following the Gill model for thermally induced circulations). The equatorial easterly moisture channel is prevailing in fall as well as in winter. The poleward branch of the moisture channel, which is associated with the anticyclonic circulation, brings moisture from TIO via the gulf of Bengal and the Maritime Continent into Southeast China and, from fall to winter shifts by about ten degrees to the east induced by planetary wave propagation.

The SST forcing experiment successfully confirms the mechanisms explaining the atmospheric responses in terms of anomalous moisture channel formation.

In summarizing, the heat induced equatorial easterly wind anomaly during the positive IOD phase transports abundant moisture from the equatorial regions westward. Its northward turn, that can be interpreted as a draw-off branch of the strong zonal-equatorial ‘moisture highway’ (double green straight arrows in Fig. 10) to South China through the Indian Ocean, North India and the Bay of Bengal, is modulated by an anticyclonic circulation anomaly over India, induced by cooling in the East Indian Ocean (Fig. 9). Consequently, the EAWM decreases which, in turn, leads to extreme precipitation events to be more likely to occur in Southeast China.

5 Conclusion

Based on daily precipitation station observations, the extreme winter precipitation in Southeast China is defined by an exceedance of the 95th percentile for each station.

The large-scale atmospheric response to SST anomalies is investigated by lagged MCA. And the features of the associated circulation fields are derived from ECMWF ERA-Interim reanalysis data by employing composite analysis. The following results are obtained:

1. The geographical distributions of extreme winter precipitation in Southeast China show a similar pattern as the distribution of general winter precipitation, with a maximum in the south of Yangtze River. On average, extreme winter precipitation contributes 20–30 % to the general precipitation in most parts of Southeast China in each winter. And on the interannual timescale the extreme winter precipitation days are highly correlated with total winter precipitation days in Southeast China.
2. Two moisture transport channels are related to the extreme winter precipitation in Southeast China: one extends from the North Indian Ocean through India and Bay of Bengal to South China, and the other from the West Pacific Ocean through Maritime Continent and South China Sea towards South China. And normal precipitation events’ circulation anomalies have similar patterns as the circulation anomalies of the extreme precipitation events, but show weaker flow intensities.
3. On the interannual timescale, ENSO (dominating the Pacific Ocean contribution) and IOD (dominating the Indian Ocean contribution) are captured in the autumn preceding the subsequent winter circulation anomalies, thereby being associated with Southeast China extreme precipitation. Contributions of ENSO and IOD could be shown separately through eliminating IOD and ENSO influences by linear regression techniques.

4. El Niño (La Niña) SST anomalies induce anticyclonic (cyclonic) circulation anomalies over the Philippine Sea, which is favorable (unfavorable) to warm and humid air transport to South China by southwesterly (northeasterly) anomalies. These circulations patterns weaken (strengthen) the northeasterlies of EAWM, leading to extreme precipitation to occur more (less) frequent in Southeast China.
5. During the positive (negative) IOD phase, abundant (fewer) moisture is transported to South China from tropical regions through North India, Bay of Bengal and Southeast Asian due to the weakened (strengthened) Walker circulations and the abnormal anticyclonic (cyclonic) circulation. They result from the abnormal SST related heating pattern with anomalous cooling (warming) in the East Indian Ocean and anomalous warming (cooling) in the West Indian Ocean in autumn, and they are maintained by warming (cooling) in the south of TIO in winter, which further decrease (increase) EAWM and results in winter extreme precipitation events more (less) likely to occur in Southeast China. Results of a numerical simulation with a GCM are in well accordance with the conclusions drawn from the ERA-Interim reanalysis.

Since at least two decades much research about direct and indirect impacts of the climate change on local weather events has been done. Although we have been focusing on observed interannual variability, there is in fact a physical link to climate change in terms of climate sensitivity via the fluctuation-dissipation-theorem applied to e.g. climate projections in the CMIP5 framework. This theorem, originally postulated to connect microscopic particle fluctuations with the macroscopic behavior of a huge number of them, gives us a tool at hand to relate internal (microscopic) variability to the probability and magnitude of (macroscopic) climate changes (Gritsun and Branstator 2007; Gritsun et al. 2008; Gershgorin and Majda 2010). That is, regions with high variability tend to react more sensitively to external excitations, such as, for example, increased net radiation. In a future study we hope to confirm this, first by testing decadal sensitivity in a control run (e.g. IPCC5 Historical run based on PI-control) and, in a second step, by a comparison of a control climate with different scenario runs. We expect an increase of the number (and perhaps the intensity) of extreme events in regions with large intra- and inter-annual variability and vice versa.

Acknowledgments This study acknowledges the support of the National Natural Science Foundation of China (41305081), National Basic Research Program “973” of China (2012CB955204), Max Planck Institute for Meteorology (MPI-M) fellowship, NUIST Scientific Funding (20110354), and Priority Academic Program Development of Jiangsu Higher Education Institutions (PAPD). We thank

Prof. Zhengyu Liu and Dr. Na Wen for inspiring discussions about statistical SST feedback pattern.

References

- Ashok K, Guan Z, Yamagata T (2001) Impact of the Indian Ocean dipole on the relationship between the Indian monsoon rainfall and ENSO. *Geophys Res Lett* 26:3001–3004
- Ashok K, Guan Z, Yamagata T (2003) A look at the relationship between the ENSO and Indian Ocean dipole. *J Meteorol Soc Jpn* 81(1):41–56
- Chou C et al (2009) El Niño impacts on precipitation in the western North Pacific-East Asian sector. *J Clim* 22:2039–2057
- Clarke AJ, Liu X (1993) Observations and dynamics of the semi-annual and annual sea levels near the equatorial Indian Ocean boundary. *J Phys Oceanogr* 23:386–399
- Czaja A, Frankignoul C (1999) Influence of the North Atlantic SST on the atmospheric circulation. *Geophys Res Lett* 26:2969–2972
- Czaja A, Frankignoul C (2002) Observed impact of North Atlantic SST anomalies on the North Atlantic oscillation. *J Clim* 15:606–623
- Dahms E, Borth H, Lunkeit F, Fraedrich K (2011) ITCZ splitting and the influence of large-scale eddy fields on the tropical mean state. *J Meteorol Soc Jpn* 89(5):399–411
- Dee DP et al (2011) The ERA-interim reanalysis: configuration and performance of the data assimilation system. *Q J R Meteorol Soc* 137:553–597
- Ding RQ, Ha K, Li JP (2010) Interdecadal shift in the relationship between the East Asian summer monsoon and the tropical Indian Ocean. *Clim Dyn* 34:1059–1071
- Dong WJ (2007) China meteorological disaster yearbook. Meteorology Press, Beijing, pp 61–68 (in Chinese)
- Feng J, Li J (2011) Influence of El Niño Modoki on spring rainfall over South China. *J Geophys Res* 116:D13102. doi:10.1029/2010JD015160
- Fraedrich K (2012) A suite of user-friendly global climate models: hysteresis experiments. *Eur Phys J Plus* 127:53. doi:10.1140/epjp/i2012-12053-7
- Fraedrich K, Jansen H, Kirk E, Luksch U, Lunkeit F (2005) The planet simulator: towards a user friendly model. *Meteorol Z* 14:299–304
- Frankignoul C, Kestenare (2005) Observed Atlantic SST anomaly impact on the NAO: an update. *J Clim* 18:4089–4094
- Frankignoul C, Chouaib N, Liu ZY (2011) Estimating the observed atmospheric response to SST anomalies: maximum covariance analysis, generalized equilibrium feedback assessment, and maximum response estimation. *J Clim* 24:2523–2539
- Gershgorin B, Majda A (2010) A test model for fluctuation-dissipation theorems with time-periodic statistics. *Physica D* 239:1741–1757
- Gill AE (1980) Some simple solutions for heat-induced tropical circulation. *Q J R Meteorol Soc* 106(449):447–462
- Gong DY, Ho CH (2002) The Siberian high and climate change over middle to high latitude Asia. *Theor Appl Climatol* 72:1–9
- Gong DY, Wang SW (1999) Long-term variability of the Siberian high and the possible influence of global warming. *Acta Geogr Sin* 54(2):125–133 (in Chinese)
- Gritsun A, Branstator G (2007) Climate response using a three-dimensional operator based on the fluctuation-dissipation theorem. *J Atmos Sci* 64:2558–2575
- Gritsun A, Branstator G, Majda A (2008) Climate response of linear and quadratic functionals using the fluctuation-dissipation theorem. *J Atmos Sci* 65:2824–2841
- Guan Z, Yamagata T (2003) The unusual summer of 1994 in East Asia: IOD teleconnections. *Geophys Res Lett* 30:1544–1547

- Huang RH, Zhou LT, Chen W (2003) The progresses of recent studies on the variabilities of the East Asian monsoon and their causes. *Adv Atmos Sci* 20:55–69
- Kim JW, Yeh SW, Chang EC (2013) Combined effect of El Niño–Southern oscillation and Pacific decadal oscillation on the East Asian winter monsoon. *Clim Dyn*. doi:10.1007/s00382-013-1730-z
- Kumar A, Jha B, Wang H (2013) Attribution of SST variability in global oceans and the role of ENSO. *Clim Dyn*. doi:10.1007/s00382-013-1865-y
- Li CY, Mu MQ (2001) The influence of the Indian Ocean dipole on atmospheric circulation and climate. *Adv Atmos Sci* 18:831–843
- Li CY, Zhou W, Wang X (2006) Decadal/interdecadal variations of ocean temperature and its impacts on climate. *Adv Atmos Sci* 23:964–981
- Li JP et al (2010) Can global warming strengthen the East Asian summer monsoon? *J Clim* 23:6696–6705
- McBride JL, Nicholls N (1983) Seasonal relationships between Australian rainfall and the southern oscillation. *Mon Weather Rev* 111:1998–2004
- Meyers G (1996) Variations of Indonesian through flow and the El Niño–Southern oscillation. *J Geophys Res* 101:12255–12263
- Philips PJ, Gill AE (1987) An analytic model of the heat-induced tropical circulation in the presence of a mean wind. *Q J R Meteorol Soc* 113:213–236. doi:10.1002/qj.49711347513
- Preisendorfer RW, Barnett TP (1983) Numerical model–reality inter-comparison tests using small-sample statistics. *J Atmos Sci* 40:1884–1896
- Rao AS, Behera SK, Masumoto Y, Yamagata T (2002) Interannual subsurface variability in the tropical Indian Ocean with a special emphasis on the Indian Ocean dipole. *Deep Sea Res II* 49:1549–1572
- Rasmusson EM, Wallace JM (1983) Meteorological aspects of El Niño/southern oscillation. *Science* 222:1195–1202
- Saji NH, Goswami BN, Vinayachandran PN, Yamagata T (1999) A dipole mode in the tropical Indian Ocean. *Nature* 401(6751):360–363
- Schmittner A, Silva TAM, Fraedrich K, Kirk E, Lunkeit F (2011) Effects of mountains and ice sheets on global ocean circulation. *J Clim* 24:2814–2829
- Shukla J, Paolino DA (1983) The Southern oscillation and long range forecasting of the summer monsoon rainfall over India. *Mon Weather Rev* 111:1830–1837
- Sun C, Yang S (2012) Persistent severe drought in Southern China during winter–spring 2011: large-scale circulation patterns and possible impacting factors. *J Geophys Res* 117:D10112. doi:10.1029/2012JD017500
- Takaya K, Nakamura H (2013) Interannual variability of the East Asian winter monsoon and related modulations of the planetary waves. *J Clim* 26:9445–9461
- Ummenhofer CC, England MH, McIntosh PC, Meyers GA, Pook MJ, Risbey JS, Gupta AS, Taschetto S (2009) What causes southeast Australia’s worst droughts? *Geophys Res Lett* 36:L04706. doi:10.1029/2008GL036801
- Vinayachandran PN, Saji NH, Yamagata T (1999) Response of the equatorial Indian Ocean to an unusual wind event during 1994. *Geophys Res Lett* 11:1613–1616
- von Storch H, Zwiers FW (1999) Statistical analysis in climate research. Cambridge University Press, 342 pp
- Walker GT (1923) Correlation in seasonal variations of weather. Part VIII: a preliminary study of world weather. *Mem Indian Meteor Dept* 24:75–131
- Walker GT (1924) Correlation in seasonal variations of weather. Part IX: a further study of world weather. *Mem Indian Meteor Dept* 24:275–332
- Wang B, Zhang Q (2002) Pacific–East Asian teleconnection. Part: How the Philippine sea anomalous anticyclone is established during El Niño development. *J Clim* 15:3252–3265
- Wang B, Wu RG, Fu XH (2000) Pacific–East Asian teleconnection: How does ENSO affect East Asian climate? *J Clim* 13:1517–1536
- Wang W, Chen X, Shi P, van Gelder PHAJM (2008) Detecting changes in extreme precipitation and extreme streamflow in the Dongjiang River basin in Southern China. *Hydrol Earth Syst Sci* 12:207–221
- Wang X, Wang DX, Zhou W, Li CY (2012) Interdecadal modulation of the influence of La Niña events on Mei–Yu rainfall over the Yangtze river valley. *Adv Atmos Sci* 29(1):157–168
- Wang B, Xiang B, Lee JY (2013) Subtropical high predictability establishes a promising way for monsoon and tropical storm predictions. *Proc Natl Acad Sci USA* 110(8):2718–2722
- Wu R, Hu ZZ, Kirtman BP (2003) Evolution of ENSO-related rainfall anomalies in East Asia and the processes. *J Clim* 16:3741–3757
- Xie SP, Hu K, Hafner J et al (2009) Indian Ocean capacitor effect on Indo–Western Pacific climate during the summer following El Niño. *J Clim* 22:730–747
- Yamagata T, Behera SK, Luo JJ, Masson S, Jury MR., Rao SA (2013) Coupled Ocean–atmosphere variability in the tropical Indian Ocean, in earth’s climate. In: Wang C, Xie SP, Carton JA (eds), American Geophysical Union, Washington. doi:10.1029/147GM12
- Yamagata T, Behera SK, Rao SA, Guan Z, Ashok K, Saji HN (2003) Comments on “dipoles, temperature gradient, and tropical climate anomalies”. *Bull Am Meteorol Soc* 84:1418–1422
- Yuan Y, Yang S (2012) Impacts of different types of El Niño on the East Asian climate: focus on ENSO cycles. *J Clim* 25:7702–7722
- Yuan Y, Yang H, Zhou W, Li C (2008) Influences of the Indian Ocean dipole on the Asian 5 summer monsoon in the following year. *Int J Climatol* 28:1849–1859
- Zhang XB, Alexander L, Hegerl GC, Jones P, Tank AK, Peterson TC, Trewin B, Zwiers FW (2011) Indices for monitoring changes in extremes based on daily temperature and precipitation data. *Wires Clim Change* 2:851–870
- Zhang L, Zhu XH, Fraedrich K, Sielmann F, Zhi XF (2014a) Interdecadal variability of winter precipitation in Southeast China. *Clim Dyn*. doi:10.1007/s00382-014-2048-1
- Zhang L, Fraedrich K, Zhu XH, Sielmann F, Zhi XF (2014b) Interannual variability of winter precipitation in Southeast China. *Theor Appl Climatol*. doi:10.1007/s00704-014-1111-5
- Zhi XF (2001) Interannual variability of the Indian summer monsoon and its modeling with a zonally symmetric 2D model. Shaker Verlag, Germany
- Zhou LT, Wu RG (2010) Respective impacts of the East Asian winter monsoon and ENSO on winter rainfall in China. *J Geophys Res* 115:D02107. doi:10.1029/2009JD012502
- Zhou LT et al (2009) Influence of South China Sea SST and the ENSO on winter rainfall over South China. *Adv Atmos Sci*. doi:10.1007/s00376-009-9102-7